Landsat Imagery from a CubeSat: Results and Operational Lessons from the R3 Satellite's First 18 Months in Space

Dee W. Pack, Garrett Kinum, Patrick D. Johnson, Timothy S. Wilkinson, Christopher M. Coffman, Cameron R. Purcell, Jon C. Mauerhan, Brian S. Hardy, Ray Russell, Kevin Mercy
The Aerospace Corporation
2310 E. El Segundo Blvd., El Segundo, CA 90245; (310) 336-5645
dee.w.pack@aero.org

ABSTRACT

R3 is a 3-U CubeSat launched on a RocketLab Electron into a 500 km circular orbit at 85° inclination on December 16th, 2018. The spacecraft flies a multispectral sensor that takes data in the six Landsat visible and near infrared bands. The R3 sensor mates a custom refractive telescope with a Materion Precision Optics Landsat filter, and an ON Semiconductor fast-framing high-sensitivity Si CMOS array, to produce 50-km wide, 44-m resolution Landsat-like image strips. Data are taken in push-broom mode and are downlinked via a 100Mbps compact lasercom system. Frames are then co-added on the ground in time-delay-integration (TDI) fashion to increase signal-to-noise ratio and create multi-spectral Earth images from the compact sensor. The system is an engineering concept demonstration of a compact multispectral sensor in CubeSat form. We describe our ConOps, flight operations, sensor focus and alignment, initial imaging check out, and initial comparisons of R3 data to Landsat-8 imagery of the same Earth locations. RGB, color infrared, and normalized differential vegetation index (NDVI) products are compared between CUMULOS and Landsat-8. Results show good multispectral image quality from the CubeSat sensor, and illustrate the ability of R3 to detect vegetation and other features in a manner similar to Landsat, as well as the challenge in perfectly exposing all 6 VIS/NIR Landsat bands using our commercial 10-bit CMOS array. We also highlight the performance of the compact laser communications system which enabled the successful performance of this mission.

INTRODUCTION

The R3 mission flies a multispectral imaging system on a 3U Cubesat. This engineering demonstration was internally funded as a pathfinder for implementing a push-broom, multi-spectral, time delay and integration (TDI) imaging system in a compact form factor. R3 was also a testbed for developing a space sensor calibration, processing, and data dissemination pipeline. In addition to the remote sensing mission objectives, demonstration and verification of the precision pointing, high throughput lasercom was a major goal.

A series of multi-mission technology demonstration CubeSats have been successfully launched and operated by the Aerospace Corporation in recent years. These projects have each built upon lessons learned from prior efforts and incorporated improvements and risk reduction for the subsystems that all satellites share: power, communications, and attitude control systems. A number of these missions were equipped with simple cameras, initially used to aid in understanding the performance of the 3-axis attitude determination and control system (ADCS) of these tiny satellites. Other cameras equipped with baffles were designed for use as star sensors, integral to improving the ADCS pointing. The ADCS evolution was essential to achieving precision pointing for lasercom, an important CubeSat mission goal first demonstrated by the NASA Optical Communication and Sensor Demonstration (OCSD) satellites, and integral to follow-on Aerospace Corporation CubeSats. The R3 effort leveraged prior flight experience with Si:CMOS sensors, and integrated a high frame rate ON Semiconductor Corporation focal plane board into a multispectral sensor payload capable of fast data readout, buffering, storage, and subsequent downlink via lasercom. The R3 imaging system may be thought of as a miniature Landsat-8 operational line imager (OLI) without the shortwave infrared (SWIR) bands. A single focal plane is mated with a Materion filter of the same design used on the Landsat-8 OLI. Earth imaging requires clocking the focal plane at a high frame rate. The frame rate is chosen to match the pixel dwell time on the ground, and timed in synch with the spacecraft orbit, so that successive pixel rows in a multi-frame collection may be co-added to build up signal-to-noise (time delay and integration). TDI imaging requires precise control of the spacecraft attitude, and makes the R3 imaging operations somewhat more complex than our prior point-and-stare imaging systems[1-3]. The sensor payload uses approximately 1.5 U of the 3U CubeSat volume, with the remainder of the spacecraft hosting the avionics, and RF and laser communications payloads. In the R3 demonstration, all of the large-area imaging data are downlinked via lasercom, and are then TDI

processed on the ground. The 100Mbps laser communications payload is a necessity in order to downlink the resulting large data volume generated by pushbroom, multispectral imaging operations. The R3 mission primary goal is demonstrating Landsat-like Earth imaging from a CubeSat platform. There were other mission objectives, involving quantitative radiometric data assessment, stellar calibration, nighttime data collection and collecting data on a wide variety of Earth scenes. Due to operational constraints, to date, R3 has accomplished only its main objective, performing the necessary on-orbit tuning collections to generate near-optimum TDI imagery examples in the 6 VIS/NIR Landsat bands. In addition, important operational lessons have been learned about: commercial focal plane performance, daytime imaging, lasercom operations, building data pipelines and georegistration, and R3 to Landsat comparison methods. The R3 spacecraft and instrument were first documented in a 2017 Small Satellite Conference paper.[4] We summarize important spacecraft and sensor details in the following section. (R3 is also referred to as AeroCube-11).

R3 Spacecraft and Payload Overview

The R3 spacecraft bus, sensor payload, mission outline, and ground calibration efforts were described in two prior papers.[4,5] The 3U bus was a two-part construction which aided in assembly and test, and was divided between payload and avionics. Approximately one half of the spacecraft volume contained the nadir-pointed multi-spectral payload and the camera board electronics, a RF antenna, and the compact lasercom payload. The laser is a 1064 nm, 2W diode-pumped Yb fiber laser with a 0.1 deg FWHM beam divergence (similar to the OCSD lasers).[6,7] The nadir face also included a small visible context camera, and a laser uplink beacon receiver for closed loop tracking, which was not utilized or needed.

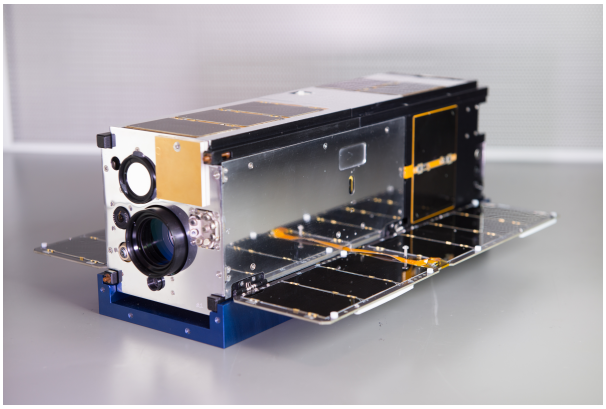

Figure 1. The Assembled R3 Spacecraft. The sunshade for the 1-inch aperture sensor is the most prominent feature on the nadir face. The shiny surface on the right is the sensor electronics radiator.

The other half of the spacecraft contained the batteries and power system, the avionics electronics stack, and included a second software defined radio (SDR) RF antenna, a GPS antenna, and two compact star sensors. The spacecraft was 3-axis stabilized and included redundant 3-axis rate gyros. Two solar wings are deployed to power the spacecraft along with the body-mounted solar panels. Pictures of the assembled R3 spacecraft nadir and zenith faces are detailed in Figures 1 and 2.

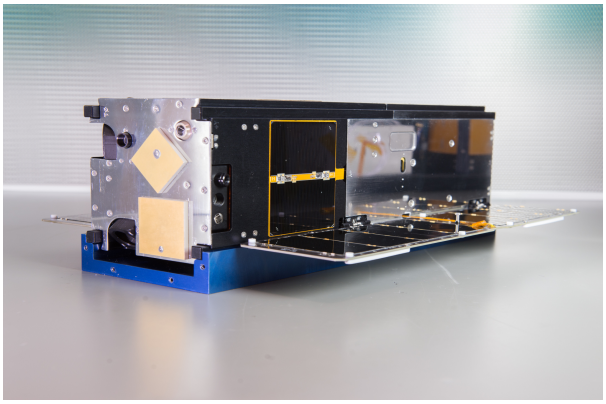

Figure 2. The Assembled R3 Spacecraft. Two patch antennas and one of the two 90° offset star sensors are prominent on the zenith face of the CubeSat.

The R3 sensor was designed to collect multispectral imagery similar to that of Landsat-8 OLI from a 3U satellite. The payload, depicted in Figure 3, consists of an Aerospace Corporation designed 1-inch refractive optical telescope paired with a commercially available ON Semiconductor LUPA 1300-2 Si:CMOS focal plane. The focal plane was chosen for its high frame rate capabilities, low noise characteristics, and our previous experience interfacing related focal plane arrays (FPA).

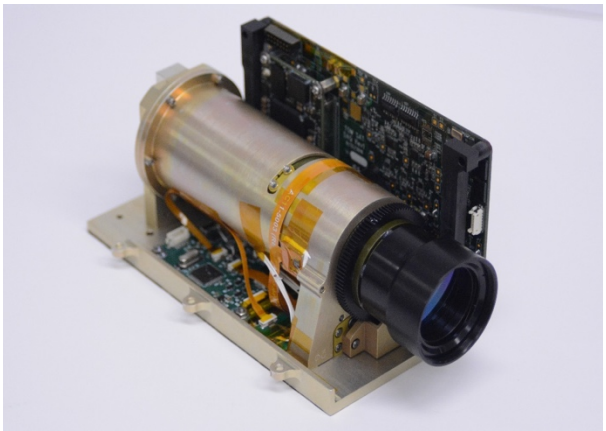

Figure 3. The R3 Sensor and Electronics.

Multispectral data were collected with a butcher block filter overlaid onto the FPA operating as a push-broom imager. The filter was provided by Materion Precision Optics and is identical to those used on Landsat-8.[4] Only the 5 visible bands and one NIR band are read out and used (Table 1). The omitted cirrus band at 1.4µm, and the two SWIR bands at 1.6 and 2.2 µm, cannot be utilized with a Si:CMOS FPA. The filter covers a subset of the FPA, and only rows actively illuminated are read out and stored, and a subset of these are coadded and processed on the ground for TDI imaging. Table 2 summarizes the sensor parameters.

Table 1: R3 Filter Wavebands

Landsat Band	Band Name	Wavelength
1	Coastal / Aerosol	0.43 – 0.45µm
2	Blue	0.45 – 0.51µm
3	Green	0.53 – 0.59µm
4	Red	0.64 – 0.67µm
5	Near Infrared	0.85 – 0.88µm
8	Panchromatic	0.50 – 0.68µm

Table 2: R3 Sensor Parameters

Sensor Specifications	R3
Lens f-number	6.4
Lens Focal Length (mm)	160
Pixel Pitch (µm)	14
Spectral Band (µm)	6 (0.43-0.89)
Quantization (bits)	10
Integration Time (ms)	~1.0 nominal, 0.1-1.8 for various daytime albedos
Frame Rate (hz)	163 (rate after on-orbit tuning)
Array Size	1280x1024 (1280x206 read out)
Nominal Alt. (km)	500
GSD (m)	44
Swath Width (km)	56

Data are buffered and then stored on an 8GB flash memory card. Further detailed description of the R3 optics and opto-mechanical design, including the telescope focus mechanism, are provided in reference 4.

R3 OPERATIONS - ON ORBIT CHECKOUT

The R3 CubeSat was launched on December 16th, 2018 on the RocketLab Electron ELaNa XIX mission, and successfully deployed into a 500 km circular orbit at 85° inclination. Contact was established on the first overpass over our groundstation network. A five-station RF ground network is currently operated by The Aerospace Corporation with ground terminals in Florida, Texas, Minnesota, California and Hawaii. This network is used for all command control and telemetry downlink via the 500kbps UHF radio (peak rate). A redundant RF radio is provided by an experimental software defined radio which increases the bandwidth by a factor of up to ten. This system has been demonstrated recently, but was not used during any of the operations described in this paper. A prototype lasercom groundstation is located in El Segundo, CA and was used for all high volume data downlink on this project.[6,7]

Checkout of the spacecraft revealed one notable ADCS anomaly, a failure of the primary rate gyro traced to likely helium contamination prior to launch. Continued operations were enabled using a backup rate gyro which was less sensitive to helium. Backup gyro performance was augmented by more frequent star tracker updates and mission functionality preserved.

Following ADCS checkout, the primary sensor was tested and found to be functional. The first Earth-pointed single frame multispectral image was taken of the Sahara Desert on 12 February, 2019. This 0.61 msec exposure showed that the sensor was working properly and the Materion filter survived launch intact. Following first light, short 10-15 frame collection sequences were used to check focus, boresight, and focal plane settings, targeting Venus, the Moon and Earth sites of opportunity with discernable features. The first pictures showed that the pre-loaded focus table based on TVAC testing was in error. Images of the moon taken at multiple focus settings, spanning the best estimate, were used to successfully anchor and correct the focus vs. temperature lookup table. The focus setting varied in a linear manner with sensor temperature, and this fix was rapidly accomplished so high quality imagery could be taken. All of these checkout images were downlinked via the UHF radio.

The lasercom system, a payload in its own right, was tested and boresighted during this same March to May, 2019 timeframe when groundstation weather allowed. The boresight tests adjust the star tracker to laser transmitter alignment. The spacecraft is pointed at the laser receive station and spiraled out from the modeled aim point. After the test, satellite telemetry and ground telescope observations are correlated to solve for the laser's alignment. This process was repeated until an acceptable boresight is achieved, and took five iterations. An example post-processed dataset is shown in Figure 4 below.

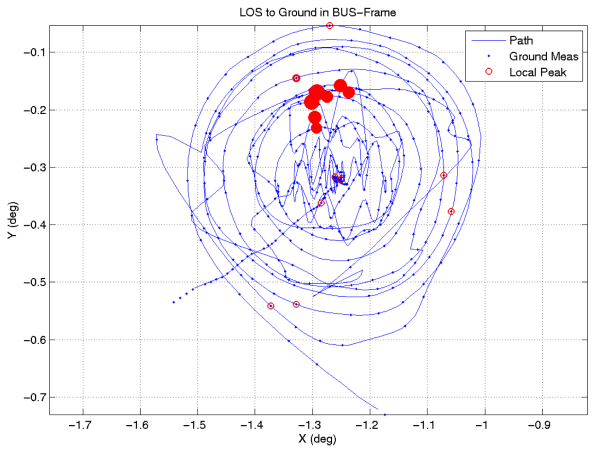

Figure 4. Post processed laser alignment scan, 0.5 degree diameter spiral. Data from 18 May, 2019.

R3 OPERATIONS - MULTISPECTRAL IMAGING

On 23 May 2019, 1000-2000 frame TDI imaging tests began with a successful collection over the South Africa-Namibia border region. Downlinking this collection did not take place until July, 2019 due to prolonged unfavorable weather at the single El Segundo, CA lasercom ground station. While not unexpected, the impact of weather highlighted the need for additional geographically diverse automated laser ground station sites, and slowed our tuning of the TDI multispectral imaging system. R3 imaging collections taken and downlinked to date are listed in Table 3.

Table 3: R3 Imaging experiments

Date Time (UT)	Location	Lat, Lon (deg.)	Int. Time (msec)	Frame Rate (hz)	Frames
05/23/19 11:32:17	Namibia/ South Africa border	-28.38, 17.40	0.85	240*	1081**
07/26/19 16:16:10	Norway	59.14, 9.71	2.5	154	1000
07/29/19 15:43:50	Greece	38.36, 22.62	2.5	180	1000
08/19/19 05:57:41	Australia	-17.67 140.65	2.5	163	1000
10/09/19 07:15:07	Greece	38.66, 21.20	2.0	165	2000
01/22/20 10:45:25	France	48.40, -4.44	2.5	163	2000***

* 180-hz intended, frame rate was set accidently high due to a software bug.

**1081 useable frames out of 2000 commanded, due to a FPGA timing error.

*** not yet downlinked due to star tracker issues. SDR will be used.

Figure 5. shows an outline of the R3 tasking, collection, processing, exploitation and dissemination (TCPED) process. The process runs through a number of steps starting with tasking.

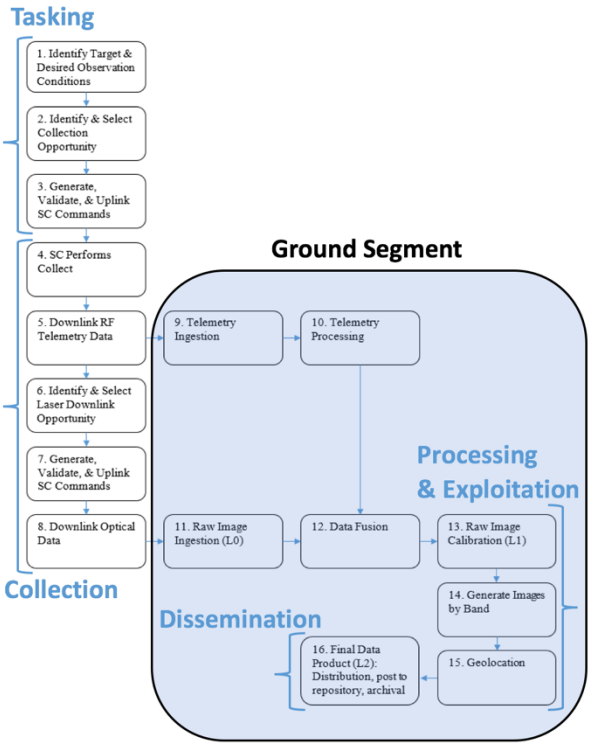

Figure 5. R3 TCPED Process.

Tasking Steps 1-3 identify sites, solar conditions desired, overflight time windows, and RF ground passes for command uplink and telemetry downlink, and then generate and execute spacecraft commands. In practice, star sensor performance determined the R3 collection opportunities. The highly compact baffles did not have the anticipated solar rejection performance, resulting in poor star detection solution rates when the nadir-to-sun angle was greater than 135 degrees. This constrained daytime imaging opportunities to certain latitudinal bands, which shifted in location and varied in extent with season and solar beta angle. Figure 6 illustrates collection opportunity zones for 22 January, 2020. On this day, favorable R3 orbital geometry enabled a Landsat equivalent time-of-day imaging opportunity over coastal Brittany in France, and data were collected. In practice, these opportunities were studied and collection sites chosen that featured coastlines, vegetated regions, and human development zones, in order to have scene features on which to tune the TDI processing and settings, until crisp imagery was generated. We describe this process in some detail below in the TDI tuning section.

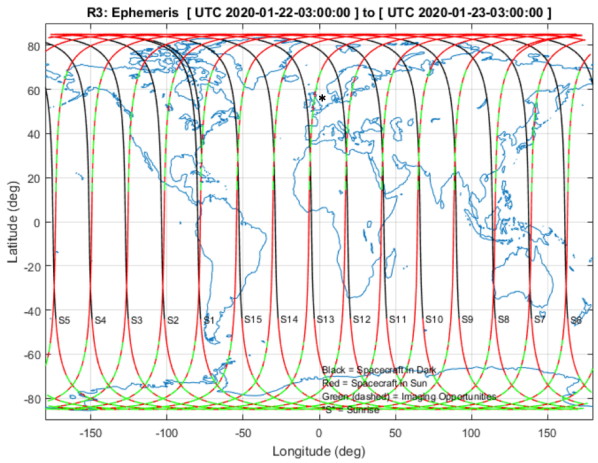

Figure 6. Example R3 imaging opportunities, green dashed lines, * marks a near conjunction), -30° beta angle.

Collection Steps 4-8 execute the imaging collect, downlink telemetry which verifys the operation, identify laser downlink opportunities, uplink the commands to execute the laser downlink, and then execute the laser pointing and transmission. While much of the ground network processing is automated, the laser downlink operations still require operator time to plan, and require staff at the prototype ground station. Nighttime weather in El Segundo made this a slow step during the summer months as late evening overpasses were clouded out. This delayed our downlinking and processing the R3 data to tune sensor settings. Figure 5 also highlights the R3 Ground Segment which is described next.

Processing, Exploitation and Dissemination Steps 9-15 include both telemetry ingest and processing, imagery ingest and parsing, fusing these two data streams, applying the radiometric calibration, multispectral imagery generation via TDI, and geolocation. The final dissemination step is populating a map-based data server with the level 2 products. Our CubeSat sensors (CUMULOS, R3 and others) are being used as test cases for building a common Aerospace Corporate data server.

A R3 Earth-pointed collection experiment begins with operators selecting a target based on location, weather and lighting conditions. Daytime operations were centered on selecting conditions that would image a target of interest under solar conditions that would not compromise the R3 star sensors as mentioned above. Developing a tasking plan takes an operator approximately two hours. Once uploaded, a collection plan takes approximately 30 minutes to execute and includes: spacecraft turn-on, ADCS initiation, commanding to nadir pointing, sensor turn-on, focus adjustment based on a temperature look-up table, and execution of uploaded, pre-programmed sensor settings at a time chosen to overfly the selected target for approximately 6-12 seconds (enough time to take 1000-2000 frames of data). Imaging is then halted and the ADCS turned off. During early operational sensor testing, fewer data frames were collected, and downlink was accomplished via the UHF radio link. Detailed tuning of the sensor and spacecraft settings required lasercom downlinking of full 1000+ frame experiments to map out approximately 56x44km areas. Single row multispectral imagery was generated and compared to the coadded TDI imagery, to determine if FPA frame rate and/or spacecraft orientation adjustments were needed. Adjusting the frame rate to match the orbital motion, and slight adjustments of spacecraft yaw orientation, proved to be necessary steps to insure the generation of unblurred TDI imagery.

R3 GROUND PROCESSING - RADCAL

Radiometric calibration was derived from ground-based measurements, but has not yet been validated on orbit using bright calibration stars. Basic dark correction, flat fielding, and non-linearity correction (small) are applied. Pre-flight radiometric calibration procedures were performed in a laboratory setting at The Aerospace Corporation during April 2017.[5] Dark frames were acquired for a range of exposure times and sensor gains appropriate for the anticipated operational settings used in space. Non-uniformity correction (flat field) frames were obtained using an integrating sphere flooded with a Welch Allyn lamp source. Sweeps of exposure time and lamp power levels (monitored by a photodiode sensor attached to one of the ports of the integrating sphere) were performed to: 1) achieve appropriate (>50%) well-fill levels in each of the filter bands, 2) test the sensor reciprocity, 3) derive non-linearity correction terms for the sensor response. These sweeps were performed for both the low and high gain settings. This was done with the goal of performing stellar calibration on orbit using high gain settings and connecting these to the low gain Earth observation settings.

Using data taken during ground calibration, sensor reciprocity was determined to be better than 2%.[5] Linearity analysis was performed on dark-subtracted and flat-fielded data. For each pixel a linear model was fit to sensor DN output as a function of recorded lamp power and divided into the data to derive the residual non-linear component of the response. For the majority of the dynamic range (20%-80% well fill) the sensor was linear to better than 10%, while stronger non-linearities were measured at levels outside of this range. The non-linear component was modeled with a cubic spline function. A data cube was created to store, for each pixel, the non-linearity correction terms of the spline curve sampled at discrete DN levels across the dynamic range. The data pipeline was constructed to interpolate a correction

factor for the data from the two nearest model spline factors on either side of the measured data value.

Radiometric calibration was intended to be performed in space using a standard star positioned at on each filter, or by observations of a Landsat calibration target. At the time of writing such observations have not yet been performed. However, counts-to-radiance conversions (in units of counts per msec per incident picowatt per pixel) can be approximated from the laboratory linearity sweeps and calibrated photodiode measurements for the following passbands: pan (59.5), blue (85.7), CA (143.2), NIR (16.2), red (48.1), green (61.0).

R3 GROUND PROCESSING - TDI PROCESSING

As mentioned above, two initial products are created from the downlinked R3 sensor data, a single-row 6-band image product, and a multi-row, TDI 6-band image product. Comparing an image generated by a single-line/frame to the multi-line/frame, TDI product was the approach we adopted for optimizing R3 pushbroom imaging performance. The first single-line image product is analogous to the output that would be produced by a single-line scanning array. The second product is the intended final output, a multi-row summation TDI pushbroom image for each of the 6 spectral bands. Here, successive scan lines are shifted and added at the same ground location to increase the signal-to-noise ratio (SNR) of the result. The number of TDI summed for each spectral band is given in Table 4 below.

Table 4: R3 TDI Lines Summed per Band

Band	1 Pan	2 Blue	3 CA	4 NIR	5 Red	6 Green
Number of TDI lines	11	19	21	21	21	21

The data processing pipeline is designed to accommodate both of these products in each of the six spectral bands. Incoming image data are organized for processing into a data cube of dimensions, samples_wide X number of spectral_data_lines X number_of_frames. Detector calibration, according to the equations described in the previous section, is then implemented prior to any product formation. Calibration is applied at the data cube level by applying a bad pixel map, followed by gain and offset correction to flat-field the sensor output. At this point, a sensor counts to radiance conversion factor may be applied for calibration. A fully processed data cube contains all of the sensor lines collected in each frame for each spectral band.

The single-line product is defined as a single image line from each spectral band at each frame time of the sensor. During ground calibration, the target output line within each spectral band was recorded. Single-line product formation for a single band consists of nothing more than extracting the given focal plane line for that band from each calibrated data frame. Data are then reformatted into a samples_wide X number_of_frames format, so that they represent a viewable image raster that can then be georegistered or further processed.

The TDI product formation is slightly more involved. For each spectral band, the focal plane lines that should contribute to the TDI sum were identified. The number of lines varies from a low of 23 to a high of 37, depending on spectral band. In principle, the ground content viewed by a particular sensor line in frame N should be exactly viewed by an adjacent line in frame N+1. This process should be repeated for each line in a given spectral band. Thus, the process of TDI summing for a given spectral band consists of summing successive lines in that band at successive frame times. The time reference for the TDI sum is chosen to be the single-line product output location. More specifically, if line N_k is the single-line product output line for band k, and $1 \leq N_k \leq TDI_k$, where TDI_k is the number of lines selected for summing in that band, then line l of the TDI output in band k is given by $D_k(1,l_{min}) + D_k(2,l_{min}+1) + \ldots + D_k(N_k,l) + \ldots + D_k(TDI_k,l_{max})$, where $D_k(i,j)$ is the ith line of band k in frame j, and the l_{min} and l_{max} are the starting and ending lines of the sum, respectively, such that $l_{max} - l_{min} + 1 = N_k$.

The band spectral filters were not installed on the focal plane such that their edges were perfectly aligned with the detector lines on the array. Instead, they were slightly canted at an angle of roughly 0.5 degrees relative to the array lines, a displacement of roughly 10 lines between samples from the first and last detector columns. In turn, this implies that in forming the TDI sum for a particular output line, not all samples across the width of the array sum over the same subset of lines. Thus, in the above expression, lmin and lmax are actually functions of the cross-array sample position, i.e., lmin = lmin(s), lmax = lmax(s), where s is the sample number across the focal plane. This construct allows flexibility to ensure that the image time associated with a particular TDI sum output line is consistent across the array.

The above summing expression depends upon successive lines at successive frame times containing the same ground samples in order to build SNR. That, in turn, depends upon the effective ground scan rate matching the sensor framing rate. The first of these was estimated prior to launch and the second was set based

on that estimate. A failure to match the frame rate to the ground scan rate results in smear, a blurring of the image.

Portions of both the single-line and TDI outputs for the first wide area image, collected near the South Africa - Namibia border on 23 May, 2019, are shown in Figure 7 below. The image has numerous terrain, river and field features suitable for imagery analysis. The small, white streaks in the single-line output are due to some blinking-like behavior on the focal plane that was uncorrected in this collect. Note, however, that it is significantly sharper than the TDI output image, which exhibits an additional blur, presumably due to a mismatch between frame rate and scan speed.

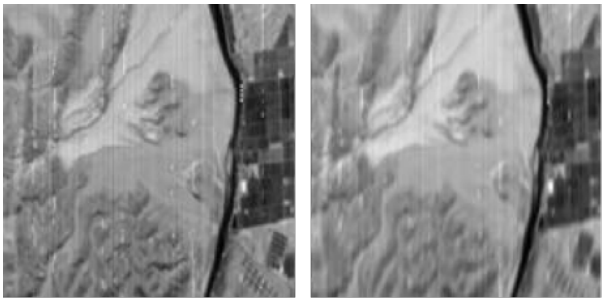

Figure 7. 23 May, 2019 11:32:17 UT, image chip comparison of panchromatic band single line to TDI processed imagery. TDI output is blurred relative to single-line product, indicating a scan velocity mismatch.

Comparisons of these two products were used to program subsequent FPA frame rates to precisely match the spacecraft motion, and to check and reprogram, if necessary, the spacecraft yaw orientation during imaging to minimize blurring along track.

By tracking the movement of image features frame-by-frame, it is possible to construct an estimate of the amount of actual velocity of scene content on the focal plane versus the desired rate of 1 GSD per frame. The plot in Figure 8 shows both the in-scan and cross-scan error in pixel motion per frame for the collection, with negative in-scan values indicating that image features are moving too slowly for the given frame rate. The sudden drops around frame number 600 are due to locations in the image in which insufficient scene content was present to make the motion estimate.

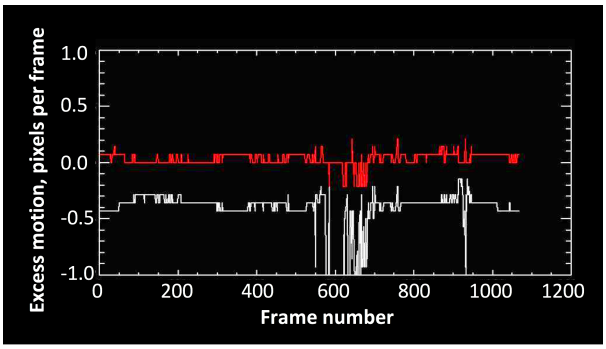

Figure 8. 23 May, 2019 image collection pixel motion analysis for in-scan (white) and cross-scan (red) directions. Data indicate that the sensor was framing too rapidly for ground motion during this collection.

Two subsequent data collections (see Table 3 above) used adjusted frames rates, and similar analysis was applied in an attempt to refine the proper frame rate value to use for the system. On 29 July, 2019, a 1000 frame image was collected over Greece at a frame rate of 180 frames/sec. The corresponding motion analysis, shown in Figure 9, indicated significant improvement relative to the first image taken. The deviations beyond line 600 are once again due to inadequate scene feature content. The cross-scan motion deviations were somewhat different than those observed in the May image. This was likely due to the analysis method itself, which: a) is prone to quantization error, and: b) used the pan band in the May example versus the green band, with a larger number of TDI, in the July example.

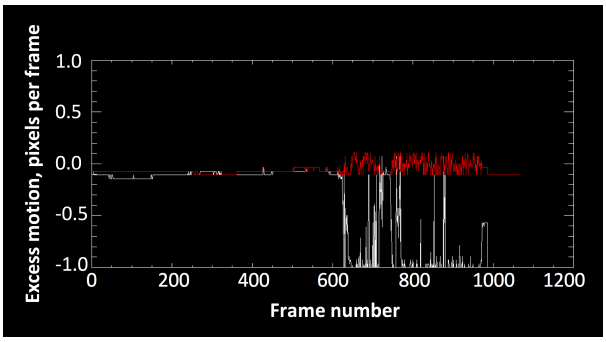

Figure 9. 29 July, 2019 image collection pixel motion analysis for in-scan (white) and cross-scan (red) directions. Data indicate that the sensor was framing too rapidly for ground motion during this collection, but less severely than in May.

Figure 10 shows a side-by-side comparison of the 6 TDI processed R3 bands from the 29 July, 2019 experiment which observed the Greek coast. These images illustrate the spectral reflectance response in the different bands, and some focal plane artifacts that showed up in the imagery. Vertical streaks sometimes appeared either

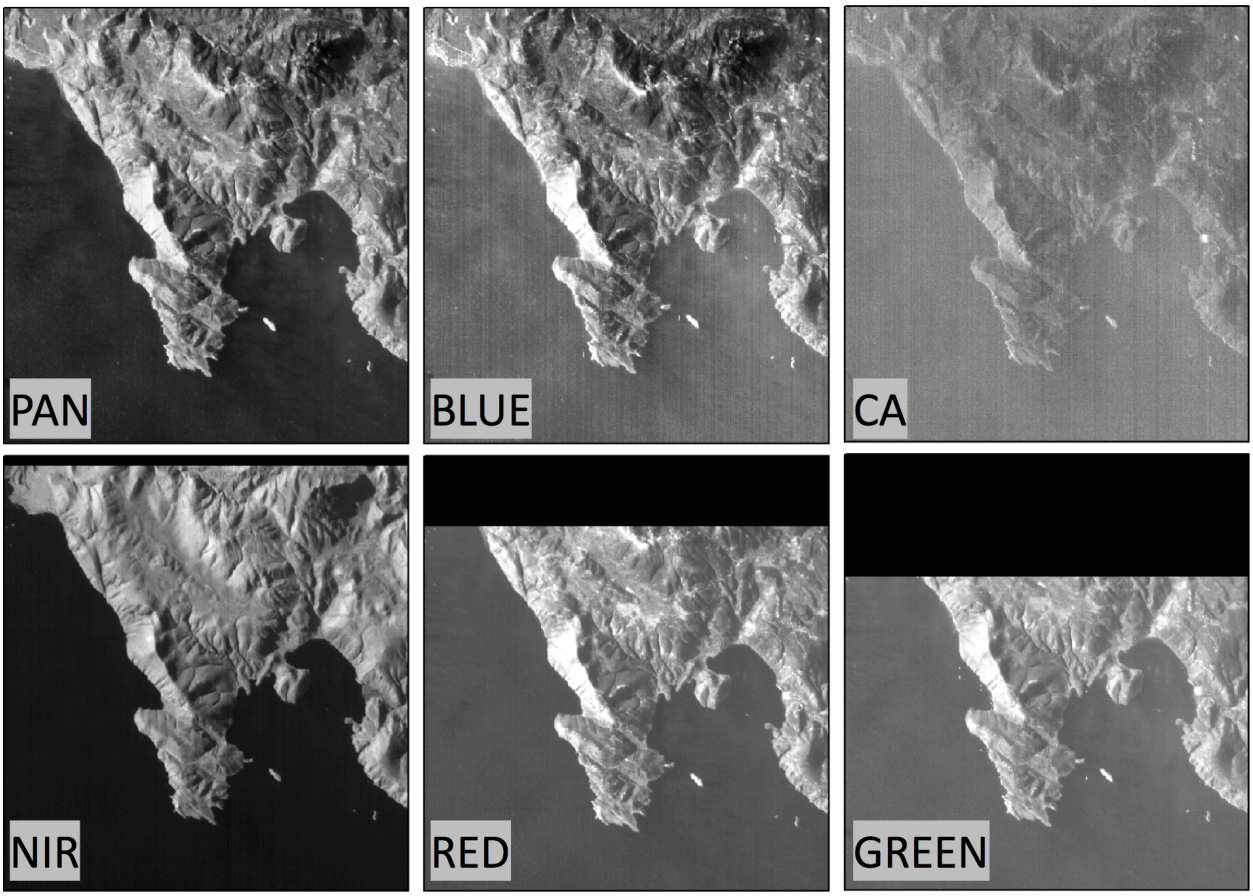

Figure 10. 29 July, 2019 15:43:50 UT, TDI processed data from all 6 R3 spectral bands imaging the coast of Greece.

randomly or along systematic columns. These were reduced by adjusting the focal plane skew settings, but not entirely removed. As discussed above, TDI was not quite optimized in this scene, but the imagery was not too blurry. For the remainder of our analysis we focus on the 19 August, 2019 1000 frame Australia data collection, which had near optimum sensor settings.

Following analysis of the 29 July data, a frame rate of 163 frames per second was recommended for the next image collection. That collection occurred on 19 August, 2019. The motion analysis, again performed on data from the green band, is shown in Figure 11. These data showed that the frame rate was just slightly too slow for the vehicle scan rate, and the correct frame rate was re-estimated at 165 frames/sec. However, the excess in-scan motion, measured at less than 1 pixel over the length of the green band TDI of 37 lines, was likely very close to the accuracy limit of the estimation method. Excess in-scan TDI smear was estimated at less than 2/3 pixel for the pan band and less than 1 pixel for the remaining bands (due to the difference in the number of TDI stages).

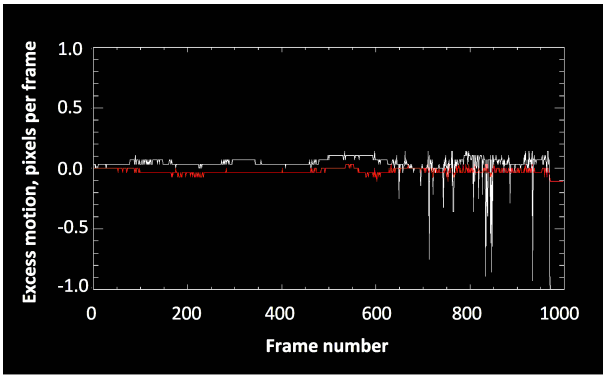

Figure 11. 19 August, 2019 image collection pixel motion analysis for in-scan (white) and cross-scan (red) directions. Data indicate that the sensor was framing slightly too slowly for ground motion during this collection.

The cross-scan motion profile in the 19 August data (in red on the plot) was very similar to that observed in the 29 July image. Together, these data indicated that the in-scan direction of the focal plane was off the ground track by an amount of less than 3 degrees. The resulting improvement in image quality is shown in Figure 12 below, in which the TDI output image has essentially the same sharpness as the single-line output. There are several features for which the apparent contrast is improved, indicating that the desired SNR gain due to TDI summing was achieved.

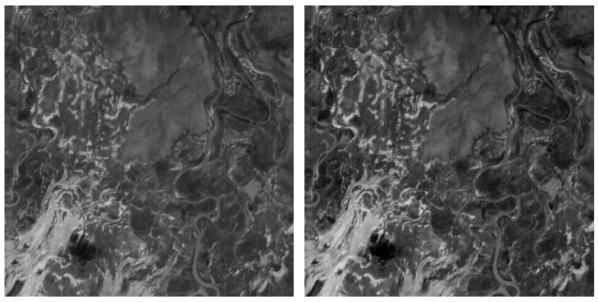

A. Single-line Green B. Full TDI Green

Figure 12. 19 August, 2019 05:57:41 UT, image chip comparison. TDI output is sharp and shows increased contrast relative to single-line output, indicating proper scan functioning.

R3 PROCESSING - GEOLOCATION & LANDSAT COMPARISON

Following the operational checkout steps and the calibration and TDI tuning described above, the R3 data were deemed ready for an initial comparison to Landsat-8 data. Reviewing the process: L0 data are radiometrically calibrated to L1. Georegistered, L1G data, are then created utilizing the sensor camera model, Earth Centered Earth Fixed (ECEF) satellite positions, and unit quaternions of orientation and rotation for each frame of data are acquired by processing the sensor ADCS data for a given collect. The ECEF positions and quaternions for each frame are tagged in the image metadata tables, and the lines of sight (LOS) for each spectral band pixel are mapped to the Earth based on its FPA central row position. Image arrays of longitude, latitude and altitude are built line by line and stored for each of the six spectral band pixels (L1G) and the satellite positions longitude, latitude and altitude are stored. A six-band, co-registered GeoTiff (L2S) for the single row and TDI image are created from the full extent of all the L1G images. For R3, the GeoTiff L2S is projected to a Universal Transverse Mercator (UTM) projection at a 40 meter ground sample distance (GSD) with six spectral bands. Since the R3 spectral bands are offset in rows on the FPA, somewhat different spatial extents are collected for each band during an image collection. In addition to the full spectral resolution L2S GeoTiff images, ancillary files are produced in R3 processing pipeline. Additional datasets are created and packaged for quick user context and local/web-based query and dissemination. Quicklook imagery, metadata, polygon shapefile of image extents and zipped archives are generated for each collected R3 image. This pipeline was developed using CUMULOS sensor data[3] prior to R3 operations beginning.

When the R3 geogregistration pipeline was implemented, minor errors were identified and traced to the calculation of the ECEF coordinates and ephemeris in the R3 meta data fields. A fix was recently implemented to correct this and further tests are planned on the georegistration pipeline. Results presented here were hand georeferenced for comparison to Landsat imagery.

Figure 13 plots the R3 red, green and blue channels overlaid on color Earth imagery. In what follows, the overlapping, hand-georeferenced portions of the R3 L2S, multispectral imagery are used for comparison to Landsat.

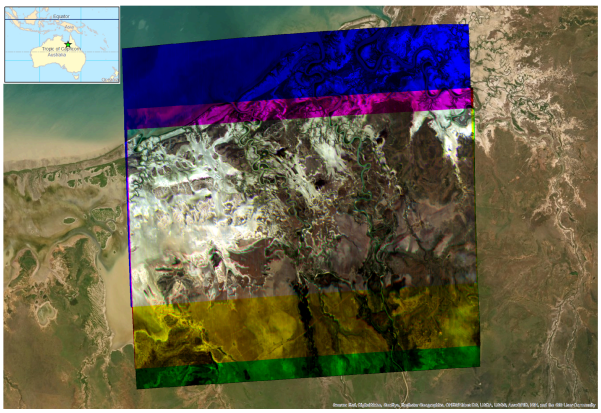

Figure 13. Overlap region of the R3 red, green and blue bands from the 19 August, 2019, 1000-frame northern Australian coast imaging experiment.

Comparisons of multi-spectral imaging products from the 19 August, 2019 Northern Australia experiment to 25 August, 2019 Landsat-8 data are provided in Figures 14 and 15. The R3 multispectral data were processed into three standard Landsat products. These are: 1) True color (which plots the red, green, and blue bands as an RGB image), 2) Color Infrared (CIR, which plots the near-IR, red, and green bands as a RGB image), and 3) normalized vegetation difference index, or NDVI. NDVI is defined by the formula: (NIR-Red)/ (NIR+Red), and varies from -1 to +1. An increase in positive values indicate the presence of vegetation. The values highlight

the strong reflectivity of plants in the NIR band and the strong absorption of Red band light. Qualitative comparison of the processed R3 data (Figure 14) to the processed Landsat-8 data (Figure 15) demonstrates the performance of the CubeSat. Following the sensor tuning experiments, the R3 system successfully collected multispectral imagery over a 56km-wide swath of diverse terrain, and generated similar products in the visible and near infrared to the larger Landsat-8 satellite. Noise in the NIR channel is noticeable and methods to mitigate this are a subject of study. A median filter was applied for cosmetic purposes. Quantitative examination of the NDVI showed that the NIR band to Red band balance was a bit off. This made the Australian saltwater estuary scene show up as somewhat "over vegetated". This is also a subject of further study. Data taken during satellite conjunctions will allow a more definitive comparison and for corrections to be made. One possibility is that tuning of the focal plane skew settings to reduce noise in the NIR band active detector rows, altered the NIR flat field (gain) performance. Correcting this would require periodic on-orbit flat field updates, or tuning using Landsat conjunctions.

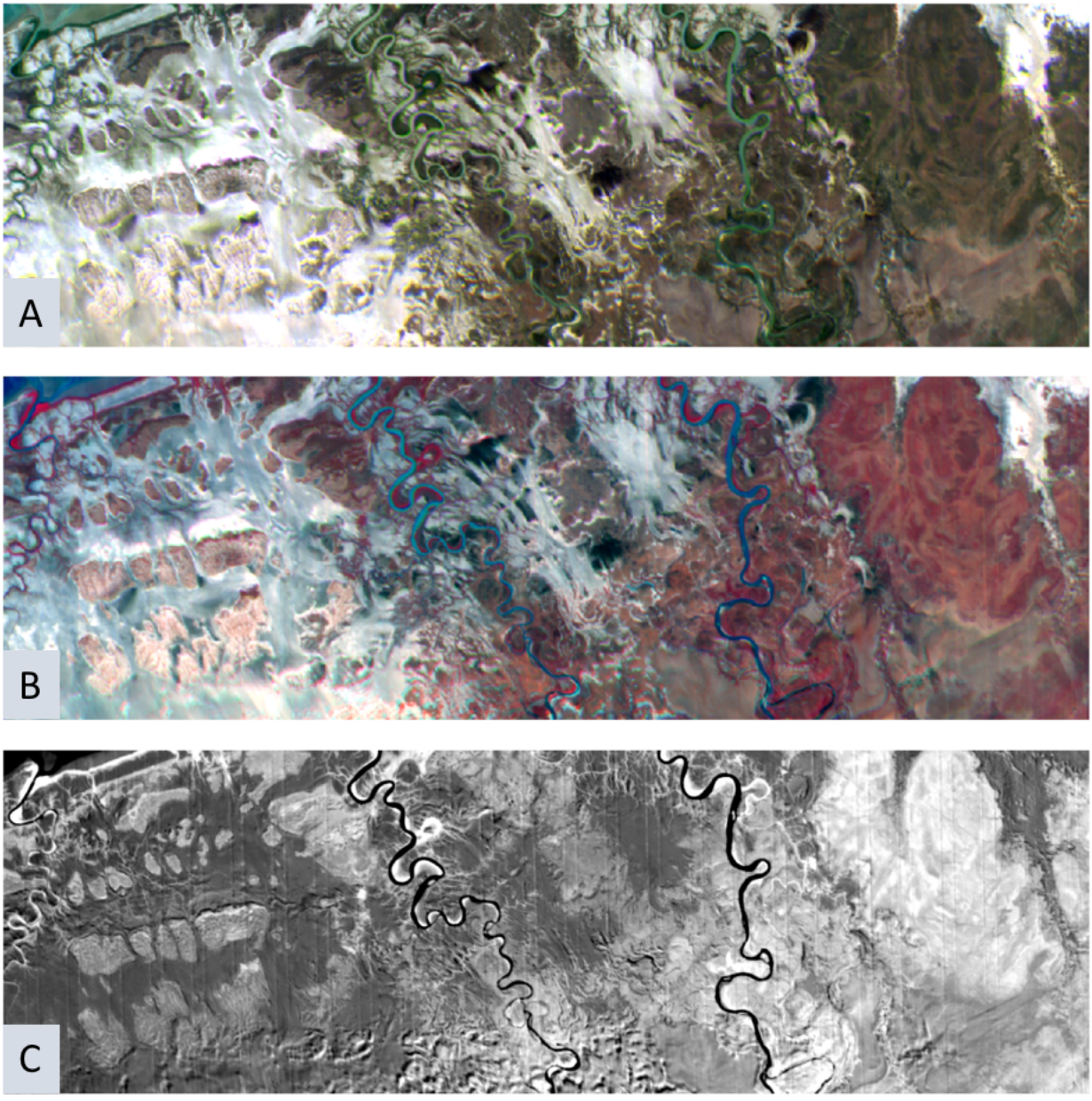

Figure 14. 19 August, 2019, 05:57:41 UT, Georegistered R3 Imagery of the Coast of Northern Australia. A) Red Green Blue imagery, B) Color Infrared, C) NDVI

When comparing the R3 and Landsat imagery, the agreement between the RGB and CIR imagery is striking. The R3 satellite's NIR channel (the Red in the CIR imagery) highlights the highly vegetated riparian areas. Likewise, the whiter high-value NDVI index highlights these same regions. Some features from solar shadows appear in the R3 afternoon collect (local time is UT + 10 hours) that do not appear in the morning Landsat data. NDVI values trended high in the R3 data, and required a small histogram offset in the displayed image to match the Landsat NDVI features detected in common, but the overall scene content is the same. Gain corrections via flat field updates, conjunction derived tuning, or both, are expected to fix this and will allow for R3 performance to be fully understood, and corrections to be implemented in the processing pipeline.

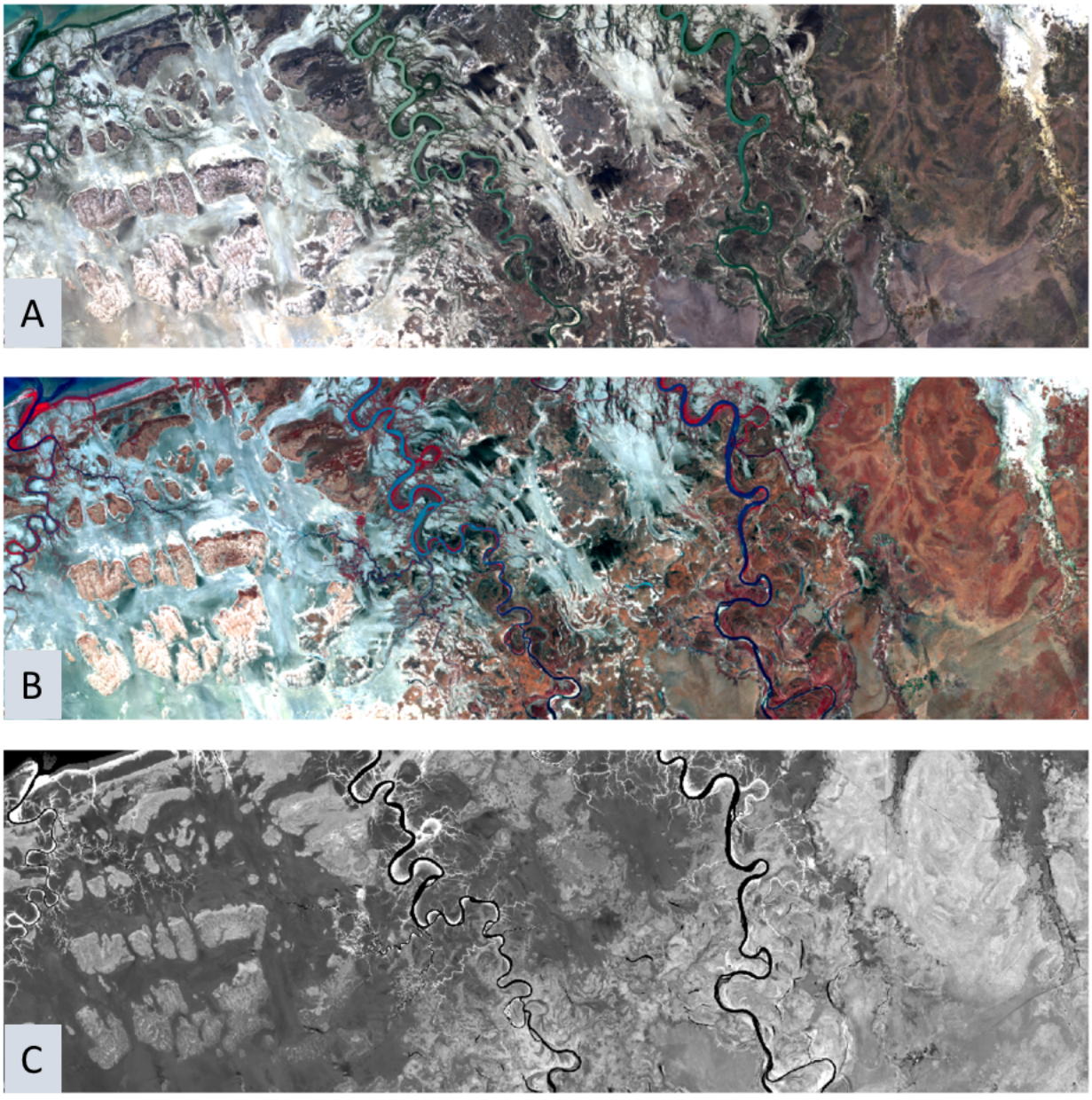

Figure 15. 25 August, 2019 00:41:18 UT Georegistered Landsat-8 data of the coast of Northern Australia. A) Red Green Blue, B Color infrared, C) NDVI. These data, taken 6 days later, were the next available cloud-free Landsat-8 imagery of the region imaged on 19 August by the R3 CubeSat. The data were taken 5 hours and 15 minutes earlier in the day as well during the usual mid-morning sun-synch. Landsat-8 overpass time.

We planned and accomplished a Landsat-8 near-conjunction collection on 22 January, 2020 over France. These R3 data have not yet been transmitted via lasercom, due to star sensor degradation issues which have made closing the laser link difficult. These data may eventually be downlinked via the experimental software defined radio which was successfully brought online during the mission. When processed, these data will allow a more definitive and quantitative comparison of the R3 radiometric performance with Landsat than the data used to date. Calculations of at-satellite radiance will be compared pixel by pixel to assess and refine the radiometric calibration of the individual R3 spectral bands. When not using conjunction data there is always the risk of weather effects, such as recent rain events, altering ratio comparisons, such as NDVI, and different solar conditions affecting the radiance values.

Conjunction experiments can be used to perform band level comparisons and update gains, if necessary. An ideal conjunction comparison would utilize data from psuedo-invarient playa sites for flat field updates, in addition to checks on diverse vegetated scenes in individual bands. Performing these experiments has been slowed due to our star-sensor imposed collection constraints and lasercom operational delays. On-orbit radiometric calibration via stellar observations is another remaining activity to be performed with the R3 multispectral sensor. This technique was pioneered for other CubeSat sensors in prior work.[3]

DISCUSSION AND CONCLUSIONS

The R3 spacecraft was built and tested as an engineering demonstration of Landsat-type multispectral imaging in a CubeSat form factor. We utilized the compact, AeroCube bus, avionics, and lasercom systems, and our multi-station ground control network, to enable our CubeSat program's first high-data-volume remote sensing mission. The mission also continued refining of our laser communications operations and procedures. The payload was a pathfinder for developing our ground calibration and data pipeline effort. Many practical lessons were learned on rapid test, on-orbit checkout and operational tasking of a small, Landsat-mimicking, push broom imaging, TDI, multispectral payload. The R3 mission combined a custom refractive telescope, feeding a surplus Landsat filter and a commercially available focal plane, into a less than 1.5U volume sensor. The small payload was able to successfully emulate the performance of Landsat's visible to near-IR wavebands, over a smaller swath width, in our initial test images.

Tasks that were underestimated for the R3 mission included: 1) the amount of time and effort desirable for ground-based testing prior to launch, 2) for follow-up in-flight calibration and validation, and 3) the degree of effort in the back-end data processing pipeline. Landsat has achieved its unprecedented continuity of mission from close attention, and large efforts, addressing all of these aspects of its land-monitoring mission. These investments are hard to duplicate in small budget satellite programs. The size of the sensor does not reduce the size of the tasks of calibrating and processing the data. Small flight sensor programs can take advantage of the Landsat program achievements, however, if cross calibration efforts are researched, put into operations and eventually automated. We hope our experience with R3 can contribute to a better understanding of how to plan and implement these types of operations. Downlinking and analyzing our already collected flight demonstration conjunction data, and, if possible, attempting the remaining stellar calibration and flat field flight test experiments, will allow us to finish refining and updating the R3 data processing pipeline.

The experience gained from the R3 program in small sensor calibration, on-orbit sensor checkout, TDI push broom imaging, data pipeline development (including georegistration), and the interplay between bus and sensor operations, has been useful to our combined engineering and science team. We are applying the knowledge gained to follow-on missions and planning for future work applying CubeSat technology to diverse remote sensing missions.

Acknowledgments

This research was funded by The Aerospace Corporation's Independent Research and Development program.

References

1. Pack, D.W., Hardy, B.S. "CubeSat Nighttime Lights" Proceedings of the AIAA/USU Conference on Small Satellites, CubeSat Session IV: LEO Missions, SSC16-WK-44. (2016). http://digitalcommons.usu.edu/smallsat/2016/S4LEOMis/1/

2. Pack, D. W., Hardy, B.S., Longcore, T., "Studying the Earth at Night from CubeSats", Proceedings of the AIAA/USU Conference on Small Satellites, CubeSat Session 10, SSC17-WK-35,(2017). https://digitalcommons.usu.edu/smallsat/2017/all2017/41/

3. Pack, D.W., C.M. Coffman, J.R. Santiago "A Year in Space for the Cubesat Multispectral Observing System: CUMULOS", Proceedings of the AIAA/USU Conference on Small Satellites, Session XI: Year in Review II SSC19-XI-01,(2019). https://digitalcommons.usu.edu/smallsat/2019/all2019/148/

4. Pack, D.W., Ardila, D.R., Herman, E., Rowen, D. W., Welle, R.P., Wiktorowicz, S.J., and Hattersley, B.W., "Two Aerospace Corporation CubeSat Remote Sensing Imagers: CUMULOS and R3", Proceedings of the AIAA/USU Conference on Small Satellites, CubeSat Session 3,SSC17-III-05.(2017). https://digitalcommons.usu.edu/smallsat/2017/all2017/82/

5. Wiktorowicz, S. J., Russell, R. W., Pack, D. W. Herman, E., Rossano, G. S., Ardila, D. R., Coffman, C. M., Hardy, B. S., Hattersley, B. W., "Calibration of the AeroCube-11 Focal Plane Array", Conf. Charact. Radiom. Calibration Remote Sens. in prep. (2017).

6. T.S. Rose, D.W. Rowen, S. LaLumondiere, N.I. Werner, R. Linares, A. Faler, J. Wicker, C.M. Coffman, G.A. Maul, D.H. Chien, A. Utter, R.P. Welle, and S.W. Janson, "Optical Communications Downlink from a 1.5U CubeSat: OCSD Program," Proceedings of the *Small Satellite* Conference, SSC18-XI-10 (2018).

7. T. S. Rose, D. W. Rowen, S. D. LaLumondiere, N. I. Werner, R. Linares, A.C. Faler, J.M. Widker, C.M. Coffman, G. A. Maul, D.H. Chen, A.C. Utter, R.P. Welle, S.W. Janson, "Optical communications downlink from a low earth orbiting 1.5U CubeSat", Optics Express, Vol. 27, No. 17, 19 Aug 2019.